Detection of neutron clusters

F. M. Marqués,[1,*] M. Labiche,[1,†] N. A. Orr,[1] J. C. Angélique,[1] L. Axelsson,[2] B. Benoit,[3] U. C. Bergmann,[4] M. J. G. Borge,[5] W. N. Catford,[6] S. P. G. Chappell,[7] N. M. Clarke,[8] G. Costa,[9] N. Curtis,[6,‡] A. D'Arrigo,[3] E. de Góes Brennand,[3] F. de Oliveira Santos,[10] O. Dorvaux,[9] G. Fazio,[11] M. Freer,[8,1] B. R. Fulton,[8,§] G. Giardina,[11] S. Grévy,[12,‖] D. Guillemaud-Mueller,[12] F. Hanappe,[3] B. Heusch,[9] B. Jonson,[2] C. Le Brun,[1,¶] S. Leenhardt,[12] M. Lewitowicz,[10] M. J. López,[10,**] K. Markenroth,[2] A. C. Mueller,[12] T. Nilsson,[2,††] A. Ninane,[1,‡‡] G. Nyman,[1] I. Piqueras,[5] K. Riisager,[4] M. G. Saint Laurent,[10] F. Sarazin,[10,§§] S. M. Singer,[8] O. Sorlin,[12] and L. Stuttgé[9]

[1]*Laboratoire de Physique Corpusculaire, IN2P3-CNRS, ISMRa et Université de Caen, F-14050 Caen Cedex, France*

[2]*Experimentell Fysik, Chalmers Tekniska Högskola, S-412 96 Göteborg, Sweden*

[3]*Université Libre de Bruxelles, CP 226, B-1050 Bruxelles, Belgium*

[4]*Institut for Fysik og Astronomi, Aarhus Universitet, DK-8000 Aarhus C, Denmark*

[5]*Instituto de Estructura de la Materia, CSIC, E-28006 Madrid, Spain*

[6]*Department of Physics, University of Surrey, Guildford, Surrey GU2 7XH, United Kingdom*

[7]*Department of Nuclear Physics, University of Oxford, Keble Road, Oxford OX1 3RH, United Kingdom*

[8]*School of Physics and Astronomy, University of Birmingham, Birmingham B15 2TT, United Kingdom*

[9]*Institut de Recherche Subatomique, IN2P3-CNRS, Université Louis Pasteur, BP 28, F-67037 Strasbourg Cedex, France*

[10]*GANIL, CEA/DSM-CNRS/IN2P3, BP 55027, F-14076 Caen Cedex, France*

[11]*Dipartimento di Fisica, Università di Messina, Salita Sperone 31, I-98166 Messina, Italy*

[12]*Institut de Physique Nucléaire, IN2P3-CNRS, F-91406 Orsay Cedex, France*

(Received 27 November 2001; published 1 April 2002)

A new approach to the production and detection of bound neutron clusters is presented. The technique is based on the breakup of beams of very neutron-rich nuclei and the subsequent detection of the recoiling proton in a liquid scintillator. The method has been tested in the breakup of intermediate energy (30–50 MeV/nucleon) ^{11}Li, ^{14}Be, and ^{15}B beams. Some six events were observed that exhibit the characteristics of a multineutron cluster liberated in the breakup of ^{14}Be, most probably in the channel $^{10}\mathrm{Be}+{}^{4}n$. The various backgrounds that may mimic such a signal are discussed in detail.

DOI: 10.1103/PhysRevC.65.044006 PACS number(s): 21.45.+v, 25.10.+s, 21.10.Gv

I. INTRODUCTION

The very light nuclei have long played a fundamental role in testing nuclear models and the underlying nucleon-nucleon interaction. While much effort has been expended in attempting to model stable systems, a number of ambiguities remain. For example, the ground states of ^{3}H and ^{3,4}He do not appear to be particularly sensitive to the form of the interaction [1]. In this context, the study of systems exhibiting very asymmetric N/Z ratios may provide new perspectives on the N-N interaction and few-body forces. In the case of the light, two-neutron halo nuclei such as ^{6}He, insight is already being gained into the effects of the three-body force [2]. Very recently, evidence has been presented that the ground state of ^{5}H exists as a relatively narrow, low-lying resonance [3]. In the case of the lightest $N=4$ isotone, ^{4}n, nothing is known [4,5]. The discovery of such neutral systems as bound states would have far-reaching implications for many facets of nuclear physics. In the present paper, the production and detection of free neutron clusters is discussed.

The question as to whether neutral nuclei may exist has a long and checkered history that may be traced back to the early 1960s [5]. Forty years later, the only clear evidence in this respect is that the dineutron is particle unstable. Although ^{3}n is the simplest multineutron candidate, the effects of pairing observed on the neutron drip line suggest that $^{4,6,8}n$ could exhibit bound states [6]. Concerning the tetraneutron, an upper limit on the binding energy of 3.1 MeV is provided by the particle stability of ^{8}He, which does not decay into $\alpha+{}^{4}n$. Furthermore, if ^{4}n was bound by more than 1 MeV, $\alpha+{}^{4}n$ would be the first particle threshold in ^{8}He. As the breakup of ^{8}He is dominated by the ^{6}He channel [7], the tetraneutron, if bound, should be so by less than 1 MeV.

The majority of the calculations performed to date suggest that multineutron systems are unbound [4]. Interestingly, it was also found that subtle changes in the N-N potentials that do not affect the phase shift analyses may generate bound neutron clusters [5]. In addition to the complexity of such *ab initio* calculations, which include the uncertainties in many-body forces, the n-n interaction is the most poorly known N-N interaction, as demonstrated by the controversy regarding the determination of the scattering length a_{nn} [8]. The

*Electronic address: Marques@caelav.in2p3.fr

†Present address: University of Paisley, Scotland.

‡Present address: University of Birmingham, UK.

§Present address: University of York, UK.

‖Present address: LPC, Caen, France.

¶Present address: ISN, Grenoble, France.

**Present address: CEA-DAM, Bruyères-le-Châtel, France.

††Present address: ISOLDE, CERN, Switzerland.

‡‡On leave from: UCL-Louvain-la-Neuve, Belgium.

§§Present address: TRIUMF, Canada.

lack of predictive power of the calculations of few-body systems at the 1 MeV level (see, for example, Ref. [9]) therefore does not exclude the possible existence of a very weakly bound ^4n.

Experimentally, no limit has yet been placed on the binding energy of ^4n (or any other ^An). Rather only limits on the production cross sections could be estimated from two-step [10–14] or direct reactions [15–21]. In this paper, a new technique to produce and detect neutron clusters is presented. The method is based on the breakup of an energetic beam of a very neutron-rich nucleus and the subsequent detection of the ^An cluster in a liquid scintillator. This work represents the continuation of an experimental program investigating the structure and, in particular, the correlations within two-neutron halo systems [22–25].

The paper is organised as follows. Section II describes the experimental technique and analysis procedures. The results, including the observation of some six events exhibiting characteristics consistent with a multineutron cluster liberated in the breakup of ^{14}Be, are presented in Sec. III. A detailed discussion of the results is given in Sec. IV. Special attention is paid to the various backgrounds (most notably pileup) that may mimic the signal arising from a multineutron cluster. Finally a summary and outlook on future work is briefly presented in Sec. V.

II. EXPERIMENTAL TECHNIQUE

A. Previous experiments

There have been essentially two categories of experiments that have searched for ^An systems. The first consists of the production of ^An in reactions such as neutron-induced fission of U [10,11] or proton and light-ion fragmentation of a heavy target [12,14]. Any recoiling ^An are then, in principle, signaled by the radiochemical separation of decay products from $(^An,xn)$ reactions in a secondary target. An extremely pure target and a detailed analysis of all possible backgrounds are thus needed. As such, only upper limits for the ^An production cross section, assuming cross sections for the $(^An,xn)$ reactions, could be determined. The only positive claim [12] was later explained as arising from an underestimation of the production of very energetic tritons [14].

The second class of experiments involves direct reactions of the type $a(b,c)^An$, where discrete values of the energy of the ejectile, c, correspond to states in the ^An system. This technique can thus also reveal unbound states. These searches have relied on the very low cross section (typically $\sim$1 nb) double-pion charge exchange (DπCX) [15–17] and heavy-ion multinucleon-transfer reactions [18–21]. Again, no conclusive evidence for a bound ^An or resonant states has been found in these studies. There are many problems inherent in this technique: precise knowledge of the many-body $(A+1)$ phase space, the background from target impurities, and the bias introduced by the fact that both the ^An *and* the ejectile have to be formed in the reaction, lowering further the production cross section.

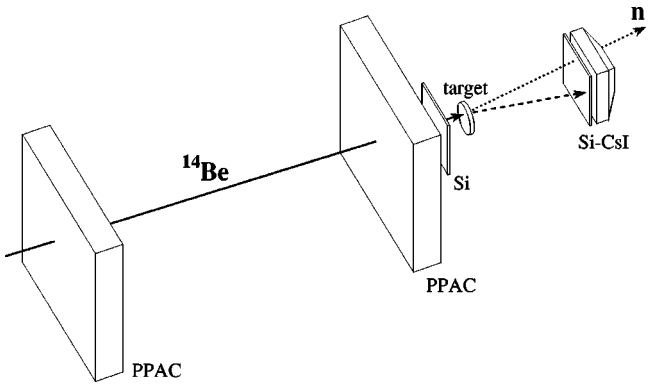

FIG. 1. Experimental setup inside the vacuum chamber. From left to right: the beam tracking detectors, the target, and the telescope for the detection of charged fragments (see text).

B. Principle

Clustering appears in many light nuclei close to particle emission thresholds [26]. Examples include $\alpha+t$ clustering in ^{7}Li (threshold at 2.5 MeV), $\alpha+\alpha+n$ in ^{9}Be ($S_n=1.6$ MeV), and $\alpha+4n+\alpha$ in ^{12}Be (threshold at 12.1 MeV). In light neutron-rich nuclei, components of the wave function in which the neutrons present a cluster-like configuration may be expected to appear [27]. Owing to pairing and the confining effects of any underlying α clustering on the protons, the most promising candidates may be the drip-line isotopes of helium and beryllium, ^{8}He ($S_{4n}=3.1$ MeV) and ^{14}Be ($S_{4n}=5.0$ MeV).

We have investigated existing data for the breakup of a 35 MeV/nucleon ^{14}Be beam by a C target [23,24,28]. Other components present in the beam which will be exploited here were ^{11}Li at 30 MeV/nucleon and ^{15}B at 48 MeV/nucleon. In such reactions relatively high cross sections (typically $\sim$100 mb) are encountered. Consequently, even only a small component of the wave function corresponding to a multineutron cluster could result in a measurable yield with a moderate secondary-beam intensity. Furthermore, the backgrounds encountered in DπCX and heavy-ion transfer reactions are obviated in direct breakup. The main difficulty in the approach lies in the direct detection of the ^An cluster.

The details of the experimental setup have been described elsewhere [23,24,28,30]. Therefore only the salient features are recalled here. The beam particles were tracked onto the breakup target (C 275 mg/cm^2) using two position-sensitive parallel-plate avalanche counters (PPACs) and identified on a particle-by-particle basis using a thin Si detector located just upstream of the target (Fig. 1). The charged fragments from breakup were detected using a position-sensitive Si-CsI telescope located at zero degrees. As discussed in Sec. III, reactions may also take place in the telescope. Importantly, the telescope, the CsI element of which was 2.5 cm thick, acted as a veto detector for any very energetic, light charged particles which may be directed towards the neutron detectors.

The neutrons liberated in breakup were detected using 90 modules of the DEMON array located at distances of 3.5–6.5 m downstream of the target [24]. The energy of the neutrons (E_n) was derived from the time of flight, with the start being furnished by the Si detector placed just forward of the

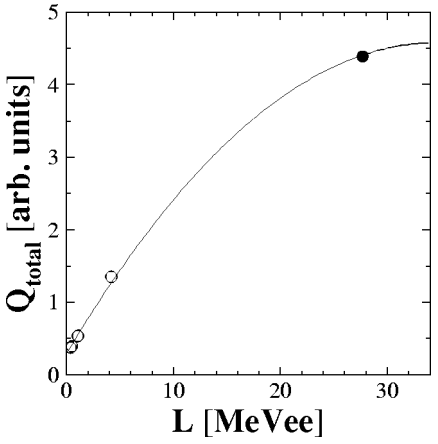

FIG. 2. Light output calibration for a DEMON module. The open symbols correspond to the Compton edge of γ rays from ^{22}Na (511 and 1275 keV), ^{137}Cs (662 keV), ^{60}Co (1333 keV), and ^{241}Am ^{9}Be (4.44 MeV) sources and the solid symbol to cosmic-ray muons [28,29]. The solid line is a parabolic fit.

target. An average resolution of 1.5 ns was obtained. For particles with $A \geqslant 2$, E_n corresponds to the energy per nucleon. Standard pulse-shape discrimination methods based on the light output from the liquid scintillator were employed to separate the neutrons from the γ- and cosmic-ray backgrounds [29]. Except where noted, only events in which a single DEMON module fired in coincidence with a charged fragment were considered in the analysis, in order to avoid any possible contributions from cross-talk [30].

The predominant mechanism for the detection of neutrons in a liquid scintillator such as that used in DEMON is *n-p* scattering [31], in which the proton recoils with an energy (E_p) up to that of the incident neutron. In general, the neutron does not lose all its energy in the interaction and may escape from the detector [30]. The energy of the recoiling proton can be determined from careful source and cosmic-ray calibrations of the charge deposited in the module [28,29,31] (Fig. 2). This may then be compared to the energy per nucleon of the incident particle derived from the time of flight (E_n). For a single neutron and an ideal detector, $E_p/E_n \leqslant 1$. For a real detector the finite resolutions can give a higher limit, and for DEMON this is $\sim$1.4. In the case of a multineutron cluster, E_p can exceed the incident energy per nucleon and E_p/E_n may take on a range of values extending beyond 1.4, as shown in Fig. 3—the scale on the upper axis indicates the maximum value as a function of the multineutron mass number.

Reactions on carbon in the liquid scintillator—as, for example, *n*-C scattering or C(n,3α)—do not present any difficulties to the present technique as the associated light outputs translate to very low E_p/E_n [31]. In addition, except for *n*-C scattering, the cross sections for reactions on C are negligible compared to scattering on hydrogen in the energy range considered here.

C. Calibrations and energy range

As is evident in the source and cosmic-ray calibrations in Fig. 2, the DEMON modules exhibit saturation effects at very high light output, as observed in earlier work [29]. It should be noted that the initial goal of the experiment run to acquire the data analyzed here was not the search for multineutron clusters, and as such the analysis of very high light outputs was not foreseen.[1] The total charge versus light output is well described up to $\sim$25 MeVee using a parabolic adjustment (Fig. 2), as found in previous tests which included measurements with a 15.5-MeV γ ray [29]. A deposited charge of $\sim$25 MeVee corresponds to a proton recoil energy of $E_p \sim 32$ MeV. In order to avoid the effects of saturation, particularly in the region $E_p/E_n > 1$, an upper limit of $E_n = 18$ MeV/nucleon has been imposed.

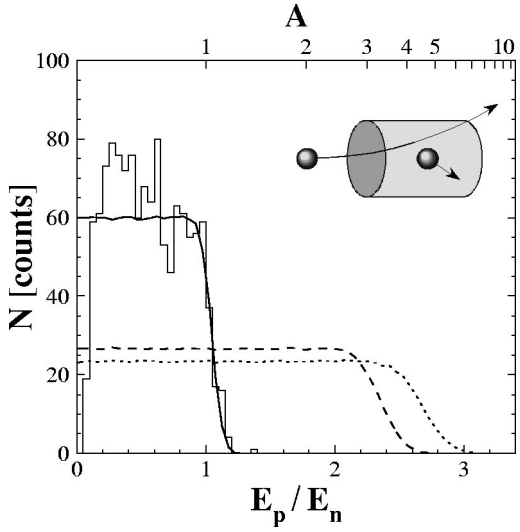

FIG. 3. Distribution of the ratio of proton energy, E_p (MeV), to the energy derived from the flight time, E_n (MeV/nucleon), for data from the reaction (^{14}Be, ^{12}Be$+n$)—histogram—and for simulations of elastic scattering of $^{1,3,4}n$—solid, dashed, and dotted lines, respectively—on protons. The experimental resolution has been included in the simulations.

At low energies the proton recoil is free of saturation effects. However, background events arising from γ and cosmic rays represent a potential contaminant of the E_p/E_n distribution. These events are randomly distributed in time, and thus the relative rate increases at low energy (Fig. 4) since $E \propto t^{-2}$. As the energy loss in a module is completely uncorrelated with the inferred time of flight from the reaction at the target, E_p/E_n is not confined below 1.4. Even if the rejection rate using pulse-shape analysis is close to 100%, any events that remain could mimic a ^{A}n signal. In order to reject these events, we have first verified that their relative rate at low energy is, as expected for a background, independent of the reaction channel (lower panel in Fig. 4). A lower limit on E_n was then imposed and raised up to the value (11 MeV/nucleon) for which no events remain in the (^{14}Be, ^{12}Be$+n$) channel, where no ^{A}n can be produced.

The energy gate, $E_n = 11-18$ MeV/nucleon, is shown as the shaded area in Fig. 4. As may also be seen in this figure,

[1]The possibility of operating the DEMON photomultipliers at lower voltages is being explored for future dedicated experiments.

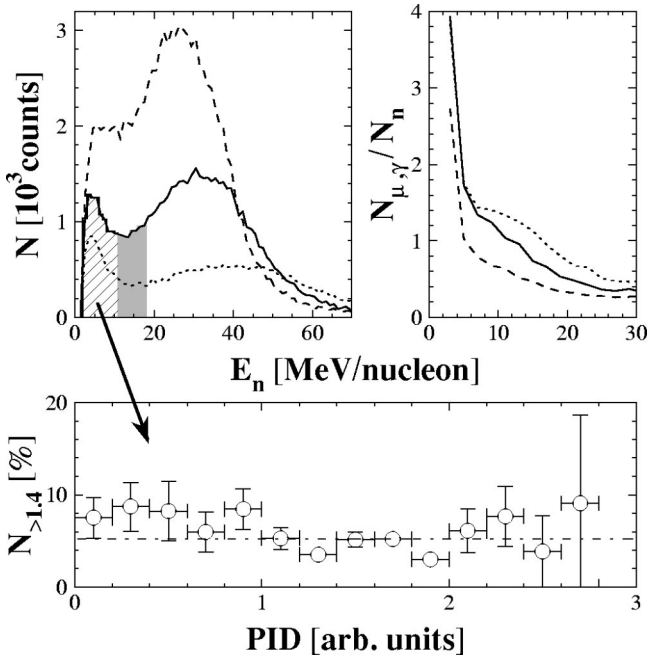

FIG. 4. Data from the reactions $(^{A}Z,X+n)$ with ^{14}Be, ^{11}Li, and ^{15}B beams (solid, dashed, and dotted lines, respectively). Left-top: neutron energy distribution; the shaded area corresponds to the energy range used in the present analysis; the percentage of events in the hatched area with $E_p/E_n>1.4$ is shown in the lower panel as a function of the particle identification parameter defined in Eq. (1). Right-top: evolution with energy of the ratio of γ- and cosmic-ray events to neutrons detected in DEMON.

the neutron energy distributions exhibit two components: the neutrons from the breakup of the projectile (distribution centered close to the beam velocity, ~30 MeV/nucleon) and low-energy neutrons evaporated by the excited target-like residue. In the case of ^{15}B, the neutrons arising from breakup are shifted to higher energies due to the higher energy of the beam, and therefore the ratio of background to neutrons is still relatively high at 11 MeV/nucleon (dotted lines in Fig. 4). A limit of $E_n=15-18$ MeV/nucleon was thus imposed for the ^{15}B data.

III. RESULTS

The detection of neutrons produced in the reaction (^{14}Be, ^{12}Be$+n$) is displayed in Fig. 3; a channel in which ^{A}n clusters should be absent. We observe that the flat distribution predicted for *n-p* scattering describes the data well, except for a small fraction of events at low E_p/E_n. As noted earlier, these correspond to reactions on ^{12}C which always generate smaller light outputs [31].

The charged fragments produced in the breakup of the beam particles were identified using the energy loss (ΔE_{Si}) and residual energy (E_{CsI}) signals derived from the telescope (Fig. 5). One-dimensional spectra representing the particle identification (PID) were constructed as [28,32]

$$\mathrm{PID}=(\Delta E_{\mathrm{Si}}+a)\exp\{-(E_{\mathrm{CsI}}-b)^2/2c^2\}. \qquad (1)$$

The PID distribution for each beam (left panels in Figs. 6 and 7) exhibits peaks corresponding to isotopes of H, He, Li, Be, and B. The parameters *a*, *b*, *c* of Eq. (1) were adjusted using the Be isotopes [28], in which the peaks corresponding to ^{10,12}Be are well resolved (Figs. 6 and 8). The cross sec-

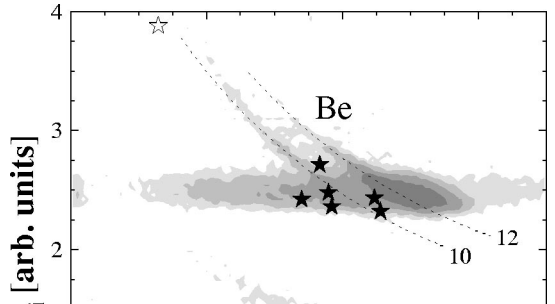

FIG. 5. Scatter plot of the energies deposited in the Si-CsI telescope for the reaction $(^{14}\mathrm{Be},X+n)$. Symbols correspond to the seven events in Fig. 6 with $E_p/E_n>1.4$. The horizontal band is discussed in the text.

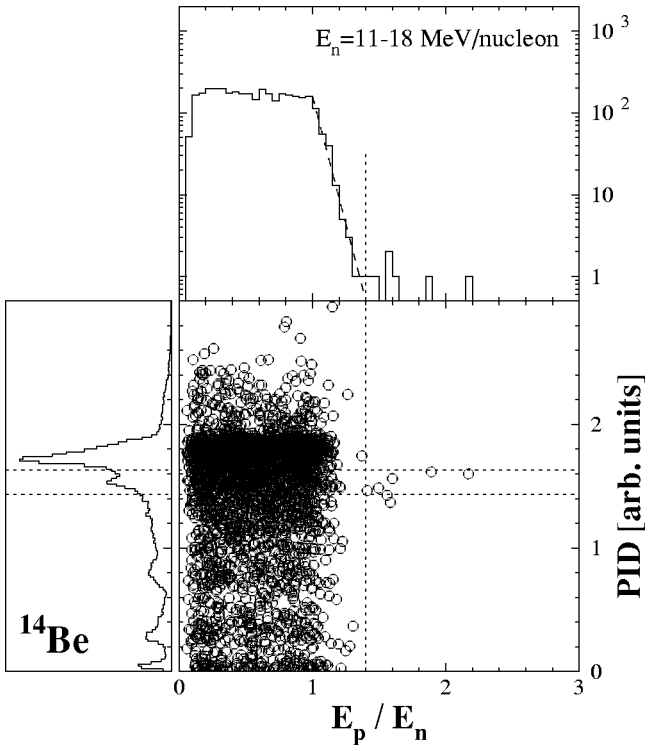

FIG. 6. Scatter plot and the projections onto both axes of the particle identification parameter PID defined in Eq. (1) vs E_p/E_n for the data from the reaction $(^{14}\mathrm{Be},X+n)$. The PID projection is displayed for all neutron energies. The dotted lines correspond to $E_p/E_n=1.4$ and to the region centered on the ^{10}Be peak.

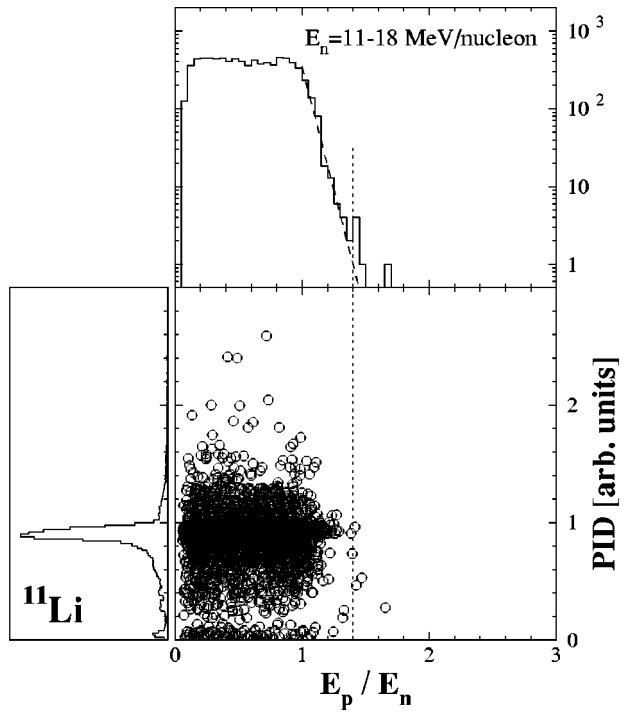

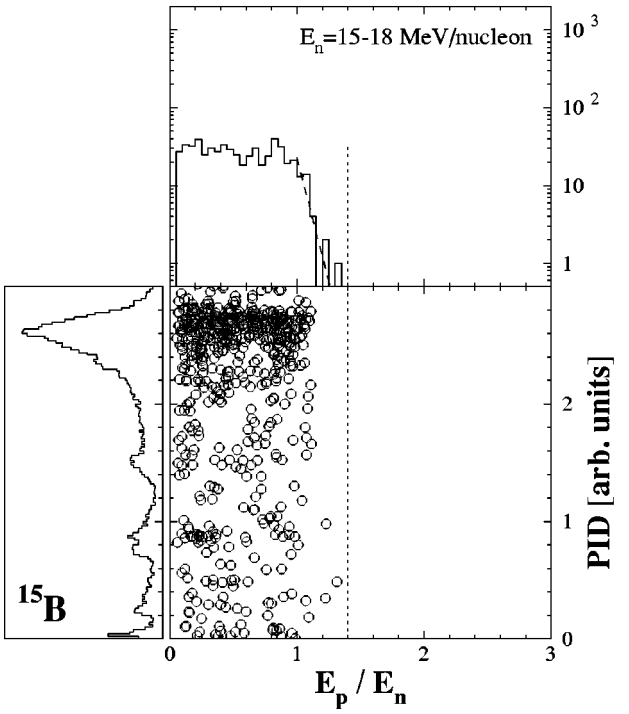

FIG. 7. Same as in Fig. 6 for the data from the reactions $(^{11}\mathrm{Li},X+n)$ and $(^{15}\mathrm{B},X+n)$.

tions for the production of ^{12,11,10}Be from the breakup of ^{14}Be were 460 ± 40, 85 ± 15, and 145 ± 20 mb, respectively [28].

The E_p/E_n distributions (upper panels in Figs. 6 and 7) exhibit a general trend below 1.4: a plateau up to 1 followed by a sharp decline, which may be fitted to an exponential distribution (dashed line). In the region where ^{A}n events may be expected to appear, $E_p/E_n>1.4$, some seven

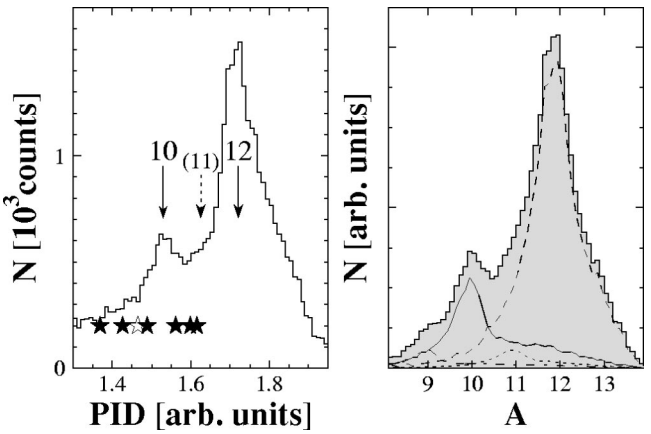

FIG. 8. Left: detail of the particle identification spectrum around ^{10,12}Be for the data from the reaction $(^{14}\mathrm{Be},X+n)$; the seven events with $E_p/E_n>1.4$ are denoted by the symbols. Right: results of the simulation described in the text for the reaction $(^{14}\mathrm{Be},^{9-12}\mathrm{Be})$; the shaded histogram is the sum of all contributions (lines).

events ranging from 1.4 to 2.2 are observed for ^{14}Be. However, in the case of ^{11}Li, despite the greater number of neutrons detected (factor of 2.4), only four events appear and lie just above threshold, while there are no events in the case of ^{15}B. Turning to the coincidences with the charged fragments produced in the breakup, the seven events produced by the ^{14}Be beam fall within a region centered on ^{10}Be. In the case of the four events produced in the reactions with ^{11}Li no similar correlation appears to exist.

The left panel in Fig. 8 displays in more detail the region of the particle identification spectrum for the breakup of ^{14}Be into lighter Be isotopes, together with the seven events for which $E_p/E_n>1.4$. Clearly, the resolution in PID does not allow us to unambiguously associate all of the observed events with a ^{10}Be fragment. However, the much higher cross section for this channel compared to ^{9,11}Be does suggest that this is the case.

The resolution of the PID distribution is in part affected by breakup reactions in the Si-CsI telescope (Fig. 1). If a ^{14}Be ion traverses the target and breaks up in the telescope, the ΔE_{Si} will correspond to ^{14}Be, but the E_{CsI} may take on a range of values depending on the depth at which the interaction takes place. Such events correspond to the horizontal band centered on $\Delta E_{\mathrm{Si}}\sim2.5$ in Fig. 5. The distribution in PID for each of the lighter Be isotopes has been studied through a simulation of breakup in all the zero-degree elements (C target plus Si and CsI detectors). The results (right panel in Fig. 8) reproduce well the characteristics of the observed PID spectrum. For each isotope, the peak corresponds to breakup of ^{14}Be in the C target, with a tail to the left owing to the energy response of the CsI. The tail to the right corresponds to the energy loss of the beam particle in the CsI before breakup: in the limiting case of ^{14}Be breakup at the end of the range in the CsI, the PID will correspond to that of ^{14}Be. Thus, while the PID are broadened by the effects of the reactions in the telescope, the seven events in question are most probably associated with a ^{10}Be fragment.

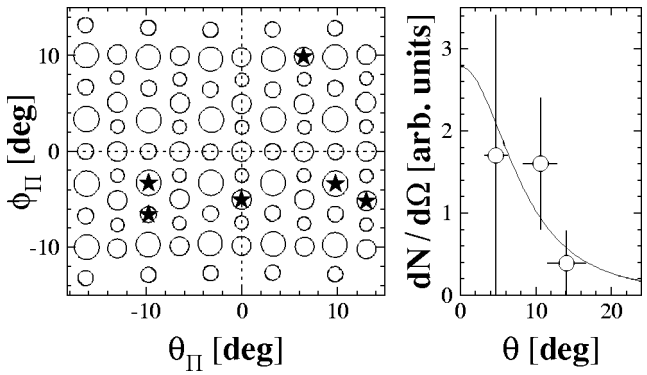

FIG. 9. Left: out-of-plane vs in-plane disposition of the DEMON modules as viewed from the target and the location of the six $^{10}\mathrm{Be}+^{3,4}n$ candidate events (symbols). Right: angular distribution.

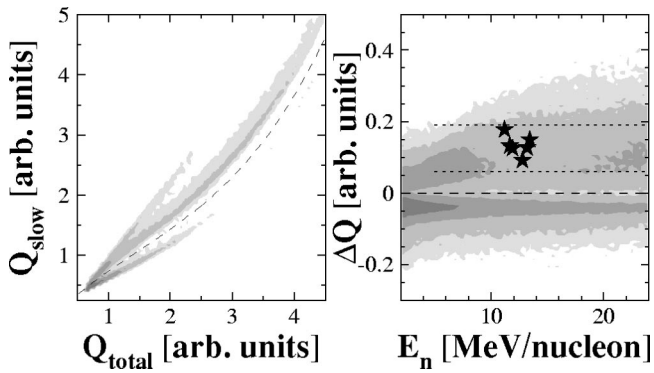

FIG. 10. Pulse-shape discrimination in DEMON for data from the reaction $(^{14}\mathrm{Be},X+n)$. Left: integrated slow component (Q_{slow}) vs the total integrated light output (Q_{total}) for a module; the dashed line separates the neutrons (upper group) and γ or cosmic rays (lower group). Right: distance in the previous plot to the dashed line as a function of the neutron energy for all modules; the symbols correspond to the six $^{10}\mathrm{Be}+^{3,4}n$ candidate events.

As a first step towards investigating the nature of these events, we have verified that each corresponds to a well-defined event in both the charged particle and neutron detectors. As described above, in terms of the charged fragment identification (Figs. 5 and 8), the seven events lie within the region corresponding to ^{10}Be. One of the events, however, exhibits a very low E_{CsI}, such that it is located well away from the region of the plot where most of the yield is concentrated. This event, with $E_p/E_n=1.41$, is denoted by the open symbols in Figs. 5 and 8. In addition, it is not kinematically consistent with the breakup of ^{14}Be into $^{10}\mathrm{Be}+^{3,4}n$, as a low-energy multineutron (11–18 MeV/nucleon) should be associated with a high-energy ^{10}Be. In the following the discussion is therefore limited to the six remaining events.

Regarding the detection using DEMON, we have checked that the six candidate events do not cluster in a single detector or group of detectors (Fig. 9). The operation of each of the detectors was then examined in detail—in particular the pulse-shape analysis. The standard procedure to select the events arising from the neutrons is to compare the integrated slow component (Q_{slow}) of the light output with the total integrated output (Q_{total}) [29]. As displayed in Fig. 10, excepting at very low Q_{total}, the neutrons form a distinct group from the γ- and cosmic-ray events. In order to present and compare the 90 modules the data have been standardized in terms of the parameter ΔQ, defined as the distance an event lies away from the line separating the two groups. The data from the 90 detectors are plotted in Fig. 10, and the six events in question are highlighted. As is clearly evident, all six events fall within the region corresponding to the detection of neutrons. In order to be sure that any possible contamination by γ- and cosmic-ray events (Sec. II) was minimal, the gate shown by the dotted lines in Fig. 10 was applied to the data.

IV. DISCUSSION

The six events in question thus exhibit characteristics consistent with detection of a multineutron cluster from the breakup of ^{14}Be. Any potential sources of events with $E_p/E_n>1.4$ not involving the formation of a multineutron are now examined in detail. Each scenario must account for the fact that the six events appear to be produced in association with ^{10}Be fragments (17% of the total yield), while no events appear in association with other fragments with comparable (H-He-Li, 19%) or higher (^{12}Be, 47%) yields.

We first address the most probable source of events, neutron pileup: i.e., the detection for the *same event* of more than one neutron in the same module. Alternative sources, including pileup of a neutron and a γ ray, the detection in DEMON of light charged particles, and the random background which was in principle rejected by the condition $E_n>11$ MeV/nucleon, are also reviewed.

A. Neutron pileup

Let us consider the possibility of pileup, or sum events [32], due to the detection of more than one neutron in the same module. As the intrinsic neutron detection efficiency is moderately low and the detector array highly granular, the pileup of just two neutrons will be the leading contribution. We define the probability of pileup leading to $E_p/E_n>1.4$ for a given channel X as

$$P_{2n}(X)=N_{2n}(X)/N(X),$$

where N is the total number of events observed for the channel $X+n$ and N_{2n} the number with $E_p/E_n>1.4$. A simple estimate of the number of events expected from pileup may be derived from channels in which no events with $E_p/E_n>1.4$ are observed. For example,

$$P_{2n}(^{12}\mathrm{Be})<1/N(^{12}\mathrm{Be}),$$

$$P_{2n}(\mathrm{H\text{-}He\text{-}Li})<1/N(\mathrm{H\text{-}He\text{-}Li}).$$

We assume that two neutrons are emitted in the ^{12}Be channel and four in the ^{10}Be one. In the latter case, therefore, there are three neutrons available to pile up. For the H-He-Li channel we assume emission of at least four neutrons. It is also assumed that the pileup distribution in E_p/E_n is flat and

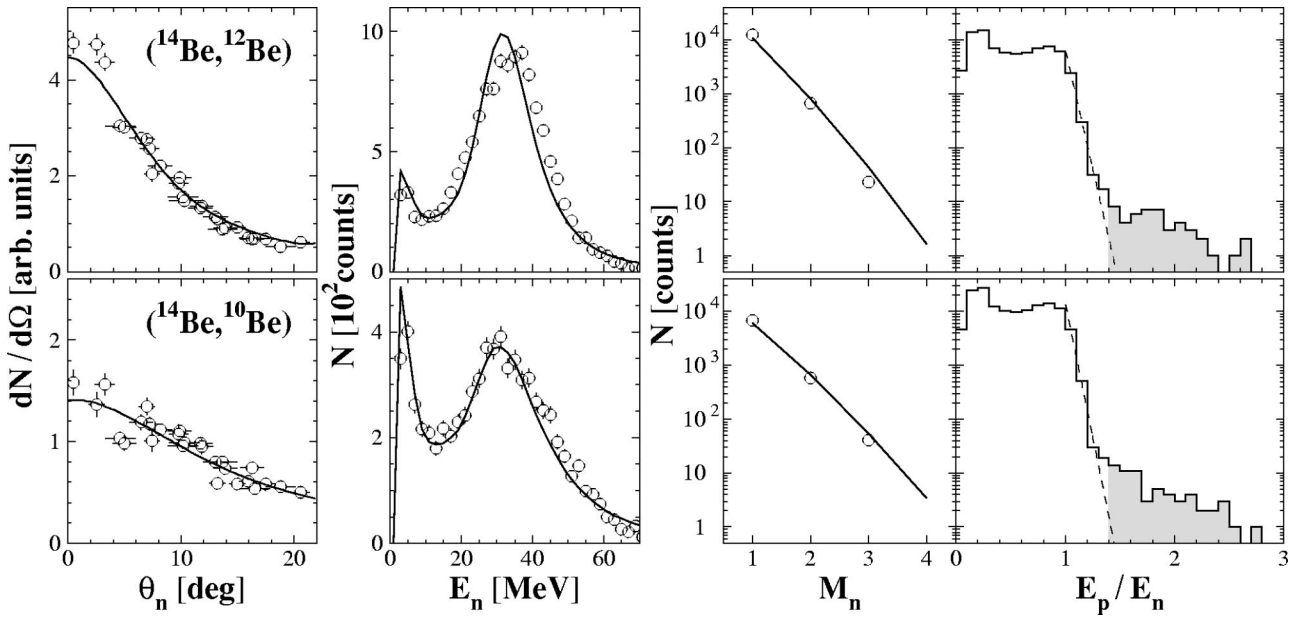

FIG. 11. Data from the reactions (^{14}Be,^{12}Be+n), upper, and (^{14}Be,^{10}Be+n), lower panels. From left to right: distributions of neutron angle, energy, and multiplicity. The open symbols are the data; the solid lines are results of the simulations described in the text. The histogram in the rightmost panel is for a simulation in which 10^7 events were generated; the dashed line is the result of a fit to an exponential for $E_p/E_n>1$.

extends up to ~3, which means that half of these events lie above $E_p/E_n=1.4$ (it will be shown below that this considerably overestimates the contribution). Therefore,

$$N_{2n}(^{10}\mathrm{Be})<N(^{10}\mathrm{Be})\times 3/2 P_{2n}(^{12}\mathrm{Be})=0.5,$$

$$N_{2n}(^{10}\mathrm{Be})<N(^{10}\mathrm{Be})\times 1/2 P_{2n}(\text{H-He-Li})=0.4.$$

At most 0.5 pileup events are expected, corresponding to a probability $P_{2n}(^{10}\mathrm{Be})\sim 9\times 10^{-4}$.

In this simple estimate we do not consider neutrons from the target nucleus, which may differ in energy, angular, and multiplicity distributions for the different reaction channels, or the non-trivial effect of the conditions applied in the analysis, such as the limits placed on the energy E_n. In order to take into account these effects and how they influence the pileup probability in each channel, a complete Monte Carlo simulation has been performed employing the code MENATE [30,33]. In the ^{10,12}Be channels, neutrons from ^{14}Be were described by an average multiplicity, with a distribution ranging from 0 to 4,2 (respectively) and a Lorentzian momentum distribution in the projectile frame with the measured width (Γ) [24,28]. For the neutrons from the target nucleus, the simulation also used an average multiplicity, with a distribution ranging from 0 up to 6, an energy distribution of the form e^{-E_n/E_0}, and a Gaussian angular distribution with a half-width $\theta_{1/2}$.

The different parameters were chosen so as to reproduce, in each channel, the measured neutron energy, angular, and multiplicity distributions. These distributions (open symbols in Fig. 11) display the main differences between the neutrons emitted in the two channels: (i) the target nucleus contribution for ^{10}Be is larger and exhibits a smaller slope, (ii) neutrons in coincidence with ^{10}Be exhibit a broader momentum distribution, and (iii) the multiplicity is higher for ^{10}Be. The simulation (solid lines), using the parameters listed in Table I, provides a good overall description of all these features.

The histograms in Fig. 11 represent the E_p/E_n distributions obtained after generating 10^7 events and applying the same analysis conditions as those applied to the data from the experiment. It should also be noted that the simulation includes the pileup arising from more than two neutrons interacting in a module. The events resulting from pileup are clearly evident for E_p/E_n above 1.4. Furthermore, as expected for pileup, the number of events decreases with increasing E_p/E_n. Interestingly, P_{2n} for the ^{10}Be and ^{12}Be channels are comparable (Table I) despite the higher multiplicity for the former—this is most probably due to the en-

TABLE I. Parameters for the simulations shown in Fig. 11: average neutron multiplicity and momentum width for the projectile-like component; average multiplicity, energy slope, and angular width for the target-like component; and the pileup probability deduced from the events within the shaded area in Fig. 11.

Channel	$\langle M(\mathrm{Be})\rangle$	Γ [MeV/c]	$\langle M(\mathrm{C})\rangle$	E_0 [MeV]	$\theta_{1/2}$ [deg]	P_{2n}
(^{14}Be,^{12}Be)	1.4	85	1.6	12	35	$(6\pm1)\times10^{-4}$
(^{14}Be,^{10}Be)	2.8	140	4.0	8	40	$(4\pm1)\times10^{-4}$

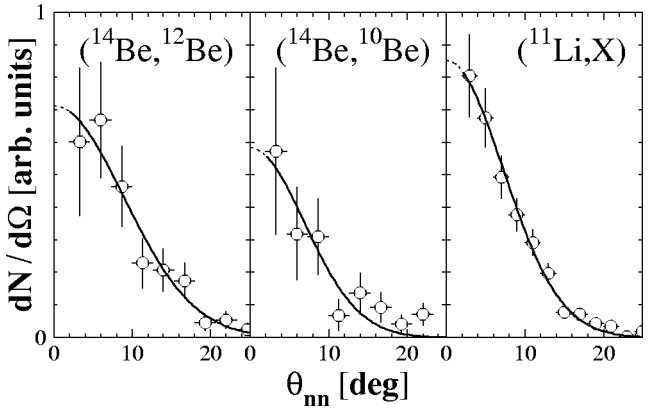

FIG. 12. Distribution of relative angle for neutron pairs from the reactions $(^{A}Z,X+2n)$ with ^{14}Be and ^{11}Li beams, selected with conditions equivalent to those used in Figs. 6 and 7. The solid line is the result of a fit to a Gaussian, which is extrapolated to $\theta_{nn}<2°$ (dotted line).

hanced forward focusing of the halo neutrons in the latter channel. The estimates lead to $N_{2n}(^{12}\mathrm{Be})=0.8$, in agreement with the experiment, and $N_{2n}(^{10}\mathrm{Be})=0.2$. Assuming $P_{2n}\sim 5\times 10^{-4}$ as an average value for the other two beams, $N_{2n}\sim 3.3$ for ^{11}Li and $N_{2n}\sim 0.3$ for ^{15}B, also in agreement with experiment.

Another estimate of pileup, which does not rely on simulations, may be made. By selecting multiplicity-2 events, the number of events in which two neutrons interact in the same detector can be deduced from the relative-angle distribution. Importantly, this approach includes explicitly all the effects arising from the different conditions applied, as the experimental distributions (Fig. 12) have been extracted under analysis conditions equivalent to those used to derive the results in Figs. 6 and 7. The distributions have been fitted according to a Gaussian line shape for $\theta_{nn}>2°$ (solid lines). The number of pairs that may be expected to be detected in a single module can now be estimated from the extrapolated fit (a single module on average subtended 1°). Using the value of the fit at 1° and assuming that half the pairs result in $E_p/E_n>1.4$, the estimated pileup probability is

$$P_{2n}(^{10}\mathrm{Be})\sim 12\times 10^{-4}.$$

It should be stressed that this estimate represents a very conservative upper limit. Even if the uncertainty of the extrapolated fit at 1° is of the order of 20% for the ^{10,12}Be channels (Fig. 12), the number of pileup events with $E_p/E_n>1.4$, as indicated by the simulations, is much less (1/3–1/6) than half the number of double hits. This method thus suggests that $N_{2n}(^{10}\mathrm{Be})<0.8$, $N_{2n}(^{12}\mathrm{Be})<1.2$, $N_{2n}<7.0$ for ^{11}Li and $N_{2n}<0.9$ for ^{15}B. These results are in line, except in the case of ^{10}Be, with the number of observed events. A summary of the different estimates of the number of pileup events is given in Table II.

B. Other sources of background

A number of other sources of background may be postulated to account for the excess of events with $E_p/E_n>1.4$.

TABLE II. Comparison of the number of events with $E_p/E_n>1.4$ for each channel with the estimated number of events expected from pileup. The methods are based on the absence of events in the ^{12}Be channel (12), Monte Carlo simulations (sim), and the relative-angle distribution of n-n pairs (nn).

Channel	N_{2n}^{expt}	$N_{2n}^{(12)}$	$N_{2n}^{(\mathrm{sim})}$	$N_{2n}^{(nn)}$
$(^{11}\mathrm{Li},X)$	4	<6.0	~ 3.3	<7.0
$(^{15}\mathrm{B},X)$	0	<0.5	~ 0.3	<0.9
$(^{14}\mathrm{Be},^{12}\mathrm{Be})$	0		0.8	<1.2
$(^{14}\mathrm{Be},^{10}\mathrm{Be})$	6	<0.5	0.2	<0.8

Above all, any such processes must account for the fact that these events appear to be correlated with a ^{10}Be fragment. One possible process that can be eliminated is the production of a large number of γ rays associated with the (^{14}Be, ^{10}Be) reaction channel. Pileup of a neutron with a γ ray could conceivably produce events with $E_p/E_n>1.4$, but the flight time for such events would be that of the γ ray and therefore the event would be rejected.

Other processes involving the detection in DEMON of charged particles not arising from reaction of the ^{14}Be beam cannot be at the origin of the events in question, as they would not give rise to a correlation with a particular channel. Light charged particles, for example, if present in the beam and yet not triggering the Si beam-identification detector or being detected in the Si-CsI telescope, should show no correlation with any particular charged fragment. In addition, such events would be concentrated very close to the beam axis, which is not the case for the six events observed here (Fig. 9).

Finally, for background events in DEMON leading to $E_p/E_n>1.4$ for an apparent $E_n<11$ MeV/nucleon (Sec. II), we have considered the correlation with the charged fragment identification (PID). The result was shown in the lower panel of Fig. 4 for the ^{14}Be beam data. The rate of events, $\sim 5\%$, is independent of the PID, suggesting that such a contamination cannot be at the origin of the observed events.

C. Kinematical constraints and properties

We have analyzed the kinematics of the six events that are consistent with the detection of a bound $^{3,4}n$ cluster. Breakup reactions in the ^{10}Be channel leading to no multineutrons, a trineutron, or a tetraneutron are

$$^{14}\mathrm{Be}^{*}\rightarrow {}^{10}\mathrm{Be}+4n \tag{2}$$

$$\rightarrow {}^{10}\mathrm{Be}+{}^{3}n+n \tag{3}$$

$$\rightarrow {}^{10}\mathrm{Be}+{}^{4}n, \tag{4}$$

with five, three, and two particles in the final state, respectively. In the average-beam-velocity frame, therefore, the relative angle (θ^{*}) between the neutron cluster detected and the ^{10}Be fragment should increase with decreasing particle number, up to a value close to 180° for reaction (4).

The experimental distributions of relative angle are shown in Fig. 13: the solid line corresponds to reaction (2), while

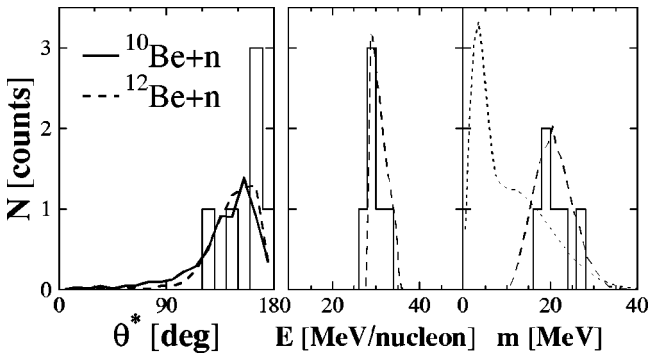

FIG. 13. Distributions for the six multineutron candidate events (histograms). Left: relative angle between the Be fragment and the neutron cluster in the average-beam-velocity frame, compared to the data for ^{10}Be+n (solid line) and to those for ^{12}Be+n (dashed line); both distributions have been normalized to six events. Middle-right: total kinetic energy and invariant mass with respect to the threshold for the ^{10}Be+^4n system; the dashed lines are the result of a simulation in which the input distribution (dotted line) has been filtered by the analysis conditions used in Fig. 6.

the dashed line is for the ^{12}Be channel, which is similar to reaction (3) in that it has three particles in the final state. Indeed, both distributions are centered at backward angles. This is due to the selection of neutrons with energies lower than the beam, as in the beam-velocity frame these always correspond to neutrons emitted backwards. However, the expected trend is observed when going from a five- to a three-particle final state, as demonstrated by the increase in the average value from $\langle\theta^*\rangle = 139°$ to 146°.

The relative angle between ^{10}Be and the neutron cluster for the six events is biased more closely to 180°, as expected for a back-to-back decay. The average value is $\langle\theta^*\rangle = 157°$. This argues in favor of reaction (4), which suggests that the most probable scenario for the events observed is the production of a tetraneutron in the breakup of ^{14}Be.

We have subsequently considered the analysis of the energies assuming that ^{10}Be+^4n breakup took place. As the tetraneutron energy has been restricted to 11–18 MeV/nucleon and the ^{14}Be beam energy is around 30 MeV/nucleon, ^{10}Be fragments in coincidence with ^4n should have energies per nucleon higher than the beam. The resulting total kinetic energy (Fig. 13, middle panel) corresponds well to the beam energy. Moreover, the reconstructed ^{14}Be* invariant mass might show strength at energies just above the ^{10}Be+^4n threshold ($S_{4n} = 5$ MeV), as was observed for ^{12}Be+2n [24]. The invariant mass distribution (Fig. 13, right panel), however, is located far above the threshold. This is related to the low-energy gating of the neutral fragment since, as noted above, the corresponding ^{10}Be fragments have high energies and thus the relative energy of the two fragments is high. This interpretation is confirmed by the dashed lines in Fig. 13, middle-right panels, which correspond to the results of a simulation of reaction (4) with a ^{14}Be invariant mass with strength at low energy (dotted line) and the low-energy gate on ^4n. They are in good agreement with the experimental distributions.

The events observed here may be used to provide estimates of the momentum content, lifetime, and production cross section of the postulated tetraneutron. A fit of the angular distribution using a Lorentzian line shape (Fig. 9) leads to a momentum width of $\Gamma = 90 \pm 60$ MeV/c. At best, it can be concluded that this is compatible with the widths measured for the single neutrons in the breakup of ^{14}Be [24,28].

Concerning the lifetime, the events observed suggest that ^4n is particle stable. However, it will be unstable against β decay because the binding energy is limited to 3.1 MeV (Sec. I), which implies [34]

$$m(^4n) - \{m(^3\mathrm{H}) + m_n\} > 6.2 \text{ MeV},$$

$$m(^4n) - m(^4\mathrm{H}) > 3.2 \text{ MeV}.$$

The average flight time of the six events from the target to DEMON is ~100 ns. This indicates that the lifetime must be of this order or longer.

The conditions applied in the analysis presented here make an estimate of the total ^4n production cross section rather difficult. Nonetheless, if we assume that the various gates affect the number of neutrons and tetraneutrons in a similar manner, we can scale the cross section measured for the production of ^{10}Be [28] by the relative yield observed and obtain $\sigma(^4n) \sim 1$ mb.

V. SUMMARY

A new approach to the production and detection of multineutron clusters has been presented. The technique is based on the breakup of energetic beams of very neutron-rich nuclei and the subsequent detection of the multineutron cluster in liquid scintillator modules. The detection in the scintillator is accomplished via the measurement of the energy of the recoiling proton (E_p). This is then compared with the energy derived from the flight time (E_n), possible multineutron events being associated with values of $E_p > E_n$.

The method has been applied to data from the breakup of ^{11}Li, ^{14}Be, and ^{15}B. In the case of the ^{14}Be beam, some six events have been observed with characteristics consistent with the production and detection of a multineutron cluster. Special care has been taken to estimate the effects of pileup. Three independent approaches were applied, and it was concluded that at most pileup may account for some 10% of the observed signal. As discussed, the most probable scenario was concluded to be the formation of a bound tetraneutron in coincidence with ^{10}Be.

The confirmation of the events observed here with a higher-intensity ^{14}Be beam and an improved charged particle identification system, and the search for similar events in the breakup of ^{8}He, appear to be the most straightforward steps to take in the near future. The saturation effects encountered with DEMON at high light outputs should be reduced considerably by lowering the beam energy and the high voltage applied to the photomultipliers. In the longer term, searches for heavier multineutron clusters may be conducted when

more neutron-rich beams become available at intensities beyond 10^2 pps.

Theoretically, multineutron clusters may provide a stringent test of our basic understanding of the nuclear interaction. If the observed events are confirmed, the challenge will become one of describing how neutron clusters may be bound. Possible avenues to such an end include advances in few-body theory, changes in parameters describing the *N-N* potential, or the introduction of new terms or many-body forces that occur in proton-free environments. Finally, the degree to which multineutron cluster-like configurations may occur in very neutron-rich nuclei will also have to be investigated.

ACKNOWLEDGMENTS

The support provided by the staffs of LPC (in particular J. M. Gautier, Ph. Desrues, J. M. Fontbonne, L. Hay, D. Etasse, and J. Tillier) and GANIL (R. Hue, C. Cauvin, and R. Alves Conde) in preparing and executing the experiments is gratefully acknowledged. This work was funded under the auspices of the IN2P3-CNRS (France) and EPSRC (United Kingdom). Additional support from the ALLIANCE program (Ministère des Affaires Etrangères and British Council) and the Human Capital and Mobility Program of the European Community (Contract No. CHGE-CT94-0056) is also acknowledged.

[1] F. Ciesielski, J. Carbonell, and C. Cignoux, Phys. Lett. B **447**, 199 (1999).
[2] M. V. Zhukov *et al.*, Phys. Rep. **231**, 151 (1993).
[3] A. A. Korsheninnikov *et al.*, Phys. Rev. Lett. **87**, 092501 (2001).
[4] D. R. Tilley, H. R. Weller, and G. M. Hale, Nucl. Phys. **A541**, 1 (1992), and references therein.
[5] A. A. Ogloblin and Y. E. Penionzhkevich, in *Nuclei Far From Stability, Treatise on Heavy-Ion Science*, edited by D. A. Bromley (Plenum, New York, 1989), Vol. 8, p. 261, and references therein.
[6] F. Ciesielski, Ph.D. thesis, Université Joseph Fourier, Grenoble, 1997.
[7] R. E. Warner *et al.*, Phys. Rev. C **62**, 024608 (2000).
[8] V. Huhn *et al.*, Phys. Rev. Lett. **85**, 1190 (2000).
[9] J. J. Bevelacqua, Phys. Rev. C **33**, 699 (1986).
[10] J. P. Schiffer and R. Vandenbosch, Phys. Lett. **5**, 292 (1963).
[11] S. Cierjacks *et al.*, Phys. Rev. **137**, B345 (1965).
[12] C. Détraz, Phys. Lett. **66B**, 333 (1977).
[13] D. Chultem *et al.*, Nucl. Phys. **A316**, 290 (1979).
[14] F. W. N. de Boer *et al.*, Nucl. Phys. **A350**, 149 (1980).
[15] J. E. Ungar *et al.*, Phys. Lett. **144B**, 333 (1984).
[16] T. P. Gorringe *et al.*, Phys. Rev. C **40**, 2390 (1989).
[17] J. Gräter *et al.*, Eur. Phys. J. B **4**, 5 (1999).
[18] G. G. Ohlsen, R. H. Stokes, and P. G. Young, Phys. Rev. **176**, 1163 (1968).
[19] J. Cerny *et al.*, Phys. Lett. **53B**, 247 (1974).
[20] A. V. Belozyorov *et al.*, Nucl. Phys. **A477**, 131 (1988).
[21] H. G. Bohlen *et al.*, Nucl. Phys. **A583**, 775 (1995).
[22] F. M. Marqués *et al.*, Phys. Lett. B **381**, 407 (1996).
[23] F. M. Marqués *et al.*, Phys. Lett. B **476**, 219 (2000).
[24] M. Labiche *et al.*, Phys. Rev. Lett. **86**, 600 (2001).
[25] F. M. Marqués *et al.*, Phys. Rev. C **64**, 061301(R) (2001).
[26] M. Freer *et al.*, Phys. Rev. Lett. **82**, 1383 (1999).
[27] Y. Kanada-En'yo *et al.*, Phys. Rev. C **60**, 064304 (1999), and references therein.
[28] M. Labiche, Ph.D. thesis, Université de Caen, 1999.
[29] I. Tilquin *et al.*, Nucl. Instrum. Methods Phys. Res. A **365**, 446 (1995).
[30] F. M. Marqués *et al.*, Nucl. Instrum. Methods Phys. Res. A **450**, 109 (2000).
[31] J. Wang *et al.*, Nucl. Instrum. Methods Phys. Res. A **397**, 380 (1997).
[32] K. Riisager *et al.*, Nucl. Phys. **A540**, 365 (1992).
[33] P. Désesquelles *et al.*, Nucl. Phys. **A307**, 366 (1991).
[34] G. Audi and A. H. Wapstra, Nucl. Phys. **A565**, 1 (1993).